

Cite this: *Phys. Chem. Chem. Phys.*, 2011, **13**, 14500–14509

www.rsc.org/pccp

PAPER

The role of disorder on the electronic structure of conjugated polymers. The case of poly-2,5-bis(phenylethynyl)-1,3,4-thiadiazole†

J.M. Granadino-Roldán,^a Nenad Vukmirović,^{bc} M. Fernández-Gómez^a and Lin-Wang Wang^{*b}

Received 8th February 2011, Accepted 19th May 2011

DOI: 10.1039/c1cp20329k

Insight into the electronic structure of disordered poly-2,5-bis(phenylethynyl)-1,3,4-thiadiazole in an amorphous region, in comparison to an ideal two-planar cofacial oligomer system, is pursued. The atomic structure of the amorphous polymer was obtained from classical molecular dynamics. It was subsequently used to calculate the electronic states and inter- and intrachain electronic coupling integrals using the density functional theory based charge patching method. The interchain electronic coupling integrals in the amorphous system were found to be an order of magnitude smaller than in the ordered system with similar distances between the chains. The results also suggest that the electronic structure of the whole system cannot be understood as a collection of the electronic structures of individual chains. The band gap of the whole system is significantly smaller than the band gaps of individual chains. This decrease originates from the disordered long range electrostatic potential created by the dipole moments of polymer repeat units, which should be minimized if one seeks good transport properties.

1. Introduction

Organic electronic materials are receiving significant attention for their potential use in a wide range of (opto)electronic applications such as light-emitting diodes (OLEDs), photovoltaic cells and field-effect transistors (OFETs).^{1,2} The performance of such devices critically depends on the rate of charge transport within the organic material.^{3,4} The mobility of the “free charge carriers” reaches as high as $75 \text{ cm}^2 \text{ V}^{-1} \text{ s}^{-1}$, as predicted in single organic crystals,⁵ which unfortunately is not practical for large scale production. On the other hand, routine fabrication techniques produce films which contain both ordered (crystalline) and disordered (amorphous) regions.⁶ Carriers in the ordered regions are delocalized and hence

highly mobile, while carrier states in the disordered regions are more localized. Whether the overall charge transport in the polymer material is mainly determined by the ordered or disordered regions depends on many factors. It often turns out that the amorphous regions actually limit the transport, as can be evidenced, for example, by quite low values of the mobility (much lower than the ones estimated for a single polymer chain or an ordered array of polymer chains). Even when the ordered domains are percolated, the connection between the domains might be amorphous. Besides, as indicated by our result, the carrier can be trapped in the disordered region. Moreover, some polymer materials even form completely amorphous structures. Therefore, the comprehension and improvement of charge mobilities in those amorphous regions would greatly contribute to widening the range of applications and raising the device efficiency.

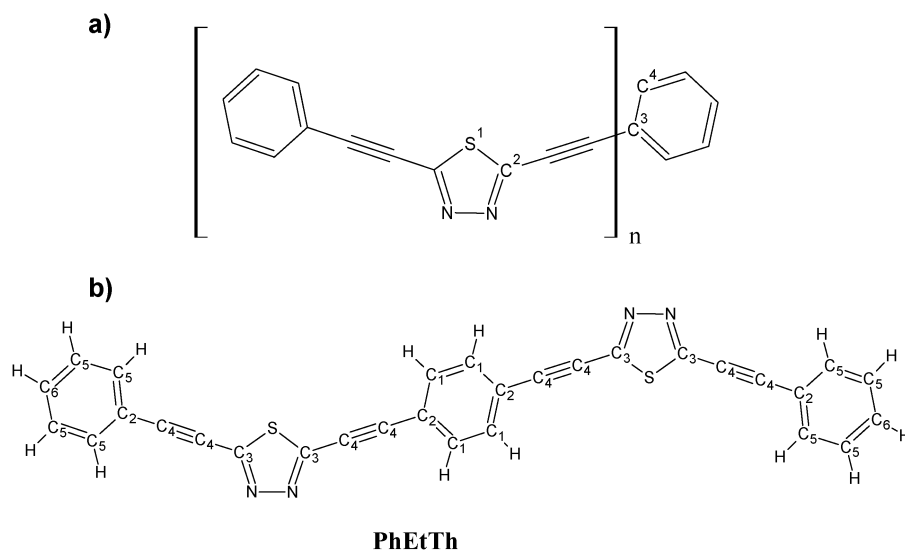
Homo- and copolymers based on conjugated heterocycles such as triazole, thiadiazole, or oxadiazole linked to phenyl units have attracted much attention as a consequence of their desirable chemical and electrical properties, *i.e.*, narrow HOMO–LUMO energy gaps, chemical and thermal stabilities, ability to inhibit corrosion, and high persistence length.^{7–11} Furthermore, when those aromatic heterocycles and phenyl units are linked through acetylene groups, the corresponding perfectly planar polymer, called poly(aryl–ethynylene) or PAE, presents a π -system which extends throughout the molecular structure. Also, as a consequence of the axial symmetry of the triple bond, the conjugation of these *molecular wires* is

^a Department of Physical and Analytical Chemistry, University of Jaén, Campus “Las Lagunillas” s/n, 23071 Jaén, Spain

^b Materials Sciences Division, Lawrence Berkeley National Laboratory, Berkeley 94720, USA

^c Scientific Computing Laboratory, Institute of Physics Belgrade, University of Belgrade, Pregrevica 118, Belgrade, Serbia

† Electronic supplementary information (ESI) available: Tables with eigenvalues and calculated band gaps for each of the chains composing the amorphous system and with highest calculated absolute interchain electronic couplings for the amorphous and perfectly planar ideal systems. Figures with the DOSs of each of the chains composing the amorphous system, and isosurface plots of the HOMO and LUMO of a planar oligomer ($n = 10$), of the LUMO+1 of the amorphous system, and of the HOMO of the amorphous system compared to the HOMO of the corresponding isolated chain. See DOI: 10.1039/c1cp20329k



Scheme 1 (a) A PhEtTh representation showing the repetitive unit and atoms involved in the inter-ring torsion modified in the force field. (b) A representation of the dimer used to extract motifs, showing the atom types used.

maintained in varying degrees between adjacent aryl groups at different relative orientations.^{12–17} On the other hand, in general, rotational barriers as small as 1 kcal mol⁻¹ have been found for PAE systems.^{15–17} These low rotational barriers imply a rather complex polymer morphology in the amorphous region and raise the questions of whether the extended π -system will persist to a certain degree, and how the amorphous region can influence electrical transport.

In previous works we have studied, from a theoretical perspective, the effect of the ethynyl group ($-\text{C}\equiv\text{C}-$) as well as the replacement of a sulfur atom by oxygen or amino NH groups on the structure and electronic properties of a PAE such as 2,5-bis(phenylethynyl)-1,3,4-thiadiazole (PhEtTh, see Scheme 1). This compound was synthesized by Yasuda *et al.* in 2005.⁷ They also reported the synthesis of a closely related polymer in which the benzene moiety includes two alkoxy substituents in *para* ($\text{OC}_{12}\text{H}_{25}$). Those studies allowed us to conclude that ideal polymeric planar chains based on PhEtTh units should behave as good n-type semiconductors, due to their predicted small band gaps, high electron affinities and low LUMO energies.^{16,17}

However, the above studies concerned only ideal infinite single chains and isolated molecules. In actual applications, what is important are the amorphous regions, which often determine the overall charge transport of the whole system. The electronic structures of the disordered amorphous regions have rarely been studied at the atomistic level, due to their high computational costs. Often, empirical assumptions for their density of states (DOS) and transport hopping rates are used in model calculations, but atomistic calculations can shed light on critical features of these systems, *e.g.*, how to control the DOS near the band edge, and what the role of disorder is in determining the electronic coupling. The electronic structure of an amorphous polymer system can be significantly different from its single straight chain or cofacial stack counter parts. It is thus not sufficient to study those ideal systems in order to deduce the electronic structure of an amorphous system.

In the current work, we will use a newly developed charge-patching method (CPM)^{18,19} to study the electronic structure of a disordered PhEtTh system containing thousands of atoms. We will study the validity of the often used assumption that the electronic structure of the whole amorphous system is the sum of its individual chains treated in isolation. We will investigate the electron coupling between chains and inside each chain. We will search for insight into what determines the DOS tails in such amorphous systems, and the role of the dipole moment in each unit of the polymer. This will be facilitated by comparison with a polythiophene polymer (without side chain) studied previously²⁰ using this method. While the polythiophene has no ring to ring dipole moment, there is a dipole moment in PhEtTh from its aromatic ring to its phenyl ring. Our results can be used as a designing principle for how to control the tail DOSs and transport properties of amorphous polymers. The current work can also serve as an additional test of the CPM for organic conjugate systems beyond polythiophenes. The CPM enables studies of systems with more than 10 000 atoms with accuracy similar to a density functional theory (DFT) calculation in a local density approximation (LDA). The atomic structure of such an amorphous region will be obtained from a classical molecular dynamics (MD) simulation.

2. Computational methods

2.1. Charge-patching method

The charge-patching method is able to produce a DFT/LDA quality charge density without actually doing a self-consistent DFT calculation.¹⁹ The charge density of a large system is obtained by adding together the charge density motifs of each atom in the system. These motifs are generated from the DFT/LDA charge density of a representative model compound. The code PETot,²⁰ with norm conserving pseudo-potentials having a kinetic energy cut-off of 60 Ry, was used to

Table 1 A list of the atom types and charge density motifs used for the charge patching of PhEtTh^a

| Atom types | Motifs |
|---|--|
| C ₁ , C ₂ , C ₃ , C ₄ , C ₅ , C ₆ , N, S, H | C ₁ -C ₂ C ₁ H, C ₂ -C ₄ C ₁ C ₁ , C ₂ -C ₅ C ₅ C ₄ , C ₃ -C ₄ SN, C ₄ -C ₄ C ₂ , C ₄ -C ₄ C ₃ , C ₅ -C ₅ C ₂ H, C ₅ -C ₆ C ₅ H, C ₆ -C ₅ C ₅ H, N-C ₃ N, S-C ₃ C ₃ , H-C ₁ -C ₂ C ₁ , H-C ₅ -C ₅ C ₂ , H-C ₅ -C ₆ C ₅ , H-C ₆ -C ₅ C ₅ |

^a A type is assigned to each atom, as indicated in Scheme 1. The notation used for the motifs implies that the central atom of the motif is specified first, followed by its nearest neighbors. If the central atom is hydrogen, next nearest neighbors have to be indicated.

obtain the DFT/LDA charge density of a prototype system made up of two unit-long oligomers ($n = 2$, see Scheme 1). The type assigned to each atom, based on its bonds and nearest neighbors, is shown in Scheme 1, while the atom types and motifs are listed in Table 1.

Once the charge density for the large system is obtained, the single-particle Hamiltonian is created by solving the Poisson equation for the Hartree potential and using the LDA formula for the exchange–correlation potential. Now, the eigenstates can be found using the folded spectrum method²¹ implemented in the ESCAN code.²² This method is particularly useful when we are only interested in a few states, 18 in this case, around the gap. It is important to emphasize that the charge-patching method scales linearly to the size of the system, while the folded spectrum method scales linearly to the size of the system and the number of states calculated.²¹ Hence, in this work we analyzed several states around the gap for systems consisting of up to 4040 atoms.

Three different systems of increasing size, for which it is still feasible to do a DFT calculation, were used to check the CPM. The charge densities obtained from direct PEtot calculations on a two unit- and a four unit-long oligomer were compared to the corresponding charge-patched densities. A snapshot from a molecular dynamics run (see below) of a system consisting of three five unit-long oligomers (321 atoms) was used to test the CPM. This test is the most clarifying one, since for the former two systems the motifs are applied to structures from which the motifs were extracted. As a consequence, the results are expected to be good. Charge patching should work in systems wherein the charge density around a given atom only depends on its local bonding environment.¹⁹ Hence, it is important to check whether this condition is satisfied in the system we intend to study. The comparison between the LDA/DFT and CPM results is summarized in Table 2. As expected, the agreement is excellent for the two and four unit-long planar oligomers, for which the differences between DFT/LDA and CPM eigenvalues amount to 22 and 33 meV for the HOMOs and 17 and 28 meV for the LUMOs of one dimer and one tetramer, respectively. In the case of the amorphous system of three twisted pentamers, the agreement is reasonably good, with differences of 150 meV for HOMOs and 42 meV for LUMOs. These differences are somewhat larger than in our

previous studies of polythiophenes.²³ First, the results for the amorphous system can be further improved by taking into account the derivative motifs²⁴ (as has been done for polythiophenes),²⁵ which describe the changes of the motifs with changes in bond lengths and angles. Second, as we will see later, the PhEtTh polymer repeat unit has a dipole moment in the direction of the polymer chain (in contrast to polythiophenes, where a repeat unit consists of two identical rings), which creates a long range electrostatic potential which may polarize the motifs. This effect can be described in terms of the polarization motifs.²⁶ For simplicity, the derivative and polarization motifs were not taken into account in the present calculation. Nevertheless, the results obtained from the CPM are still highly satisfactory, as can also be seen from the comparison of the DOSs obtained from CPM and DFT/LDA, for the three five unit-long oligomer amorphous system, shown in Fig. 1.

2.2. MD Simulations

The amorphous region of a polymer obtained from a PhEtTh building block has been studied from a classical MD simulation with periodic boundary conditions. We initially chose a system composed of five chains, each one having $n = 10$ units. Those chains were randomly placed in a cubic box whose dimensions were significantly larger than the dimensions of the box corresponding to the natural density of the system. A $100 \times 100 \times 100 \text{ \AA}^3$ box was used, and a temperature of 1000 K, significantly higher than the room temperature, was imposed. The system is allowed to equilibrate for 100 ps at that temperature under the NVT ensemble, and afterwards it is cooled down from 1000 to 300 K over 200 ps. Later on, the initial box is compressed to a $20 \times 20 \times 20 \text{ \AA}^3$ box at 300 K and the ensemble is afterwards changed to isotropic NPT ($P = 1 \text{ atm}$) in order to let the system to relax and determine the final box size. After a 1.1 ns MD run under the NPT ensemble, the final box size became $25.3 \times 25.3 \times 25.3 \text{ \AA}^3$, implying a predicted density of 1.107 g cm^{-3} . This step is followed by an equilibration over 300 ps at constant volume and a final relaxation to a local minimum. This protocol, similar to other MD-based methods used for the generation of amorphous atomic structures,^{27,28} allows the system to explore a significant amount of conformational

Table 2 Comparison between DFT/LDA and CPM results

| | % charge density difference | E_{HOMO} (eV) | | E_{LUMO} (eV) | |
|-------------|-----------------------------|------------------------|--------|------------------------|--------|
| | | DFT/LDA | CPM | DFT/LDA | CPM |
| 1 dimer | 0.17 | -4.451 | -4.429 | -2.479 | -2.462 |
| 1 tetramer | 0.18 | -4.620 | -4.587 | -2.852 | -2.824 |
| 3 pentamers | 0.96 | 5.916 | 6.064 | 7.540 | 7.498 |

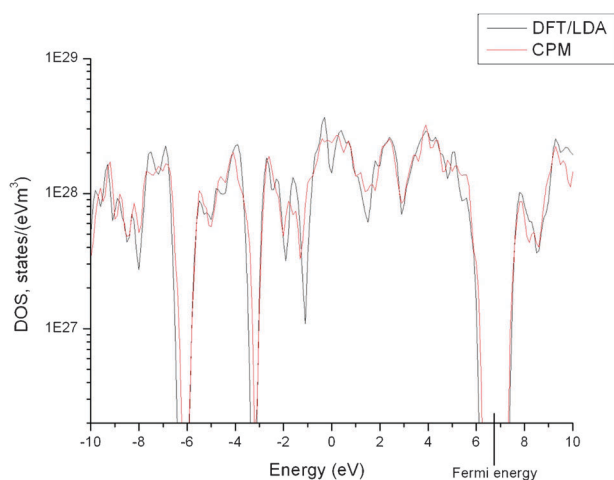


Fig. 1 The dependence of the density of states (states/eV m³, logarithmic scale) on energy using DFT/LDA density and CPM density.

space, preventing it from being trapped in a local minimum which would highly depend on the random initial conditions.

MD simulations were performed using the LAMMPS code²⁹ together with the class II polymer consistent force field (PCFF).³⁰ Unfortunately, similarly to that reported for polythiophenes,²³ the force field torsion parameters were not able to properly describe rotations of the phenyl and thiadiazole rings around the ethynyl moiety (torsions defined by atoms 1–2–3–4, see Scheme 1). These torsions are crucial for determining the overall shape of the chains and consequently the electronic structure. Therefore, the torsional potential profile was extracted from a relaxed B3LYP/6-31G* calculation¹⁶ The calculated B3LYP/6-31G* relaxed torsional profile, which takes the form $E = 0.576 [1 - \cos(2\phi)]$ kcal mol⁻¹ (ϕ represents the dihedral angle defined by atoms 1–2–3–4, see Scheme 1), was then added to the force field. The relaxed bond lengths and angles used in the force field were also extracted from B3LYP/6-31G* calculations, while the other parameters of the force field were not changed (see ESI† for full details).

2.3. Interchain and intrachain coupling integrals

The electronic coupling between the different chains and the evolution of the electronic structure from a single chain to an amorphous system has been assessed through the coupling integrals defined as:²

$$t_{ij} = \langle i | H | j \rangle \quad (1)$$

where H is the single-particle Kohn–Sham Hamiltonian of the whole amorphous system, while $|i\rangle$ and $|j\rangle$ are the eigenstates of a single chain (under H_{single} , in the absence of other chains, which is calculated also by CPM). $|i\rangle$ and $|j\rangle$ could belong either to different chains (interchain coupling integrals) or to the same chain (intrachain coupling integrals). Since the eigenstates of different chains are not strictly orthonormal; the coupling integrals calculated according to eqn (1) would depend on the choice of reference energy (an overall constant energy shift from H). To avoid this issue, we have first orthonormalized, using Löwdin's orthonormalization procedure,³¹ the set of states consisting of eigenstates of individual chains.

The coupling integrals were then calculated based on the orthonormalized states.

3. Results and discussion

3.1. Determination of the initial amorphous model

Since one of the aims of this work is to describe the properties of an infinite amorphous PAE system, an issue to be solved is determining an appropriate, representative, size for the system. An initial system consisting of five chains, each one being ten units long (1010 atoms in total), was chosen and subjected to the previously described MD protocol. In order to check that the chosen system size was big enough to reproduce the properties of an infinite amorphous material, a system consisting of 20 oligomers, each being 10 units long (4040 atoms in total), was also considered. For this latter system, we followed a similar MD protocol, starting this time with 20 chains randomly placed in a $400 \times 400 \times 400 \text{ \AA}^3$ box, and chose a final cubic box size of $40.182 \times 40.182 \times 40.182 \text{ \AA}^3$ to obtain a density of

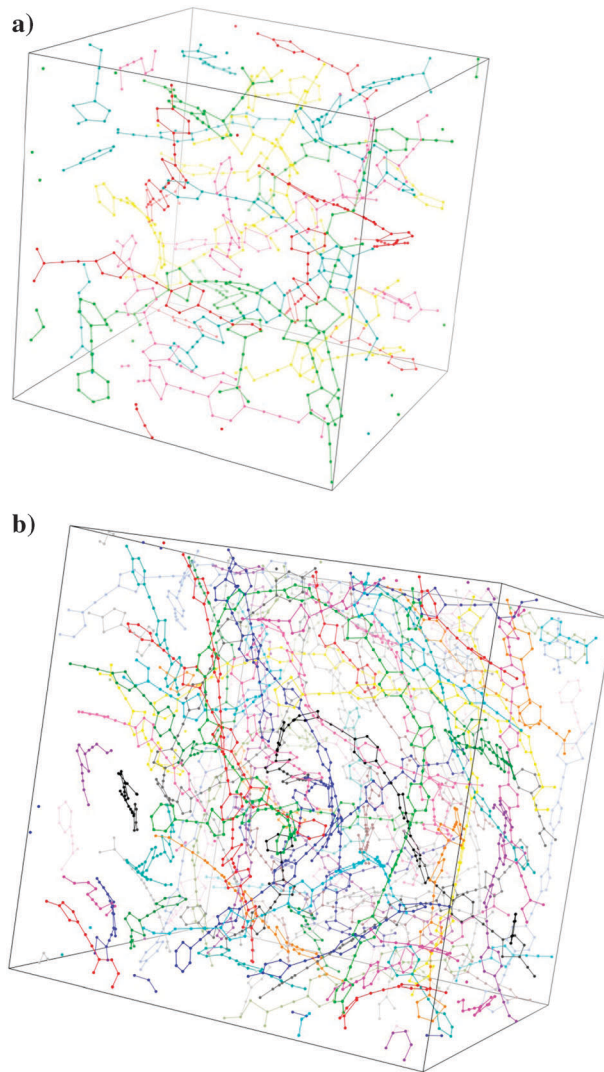


Fig. 2 Atomic structures in the case of (a) 5 decamers and (b) 20 decamers. Each chain has a different colour and the repetitive box is outlined. Hydrogen atoms have been removed for clarity.

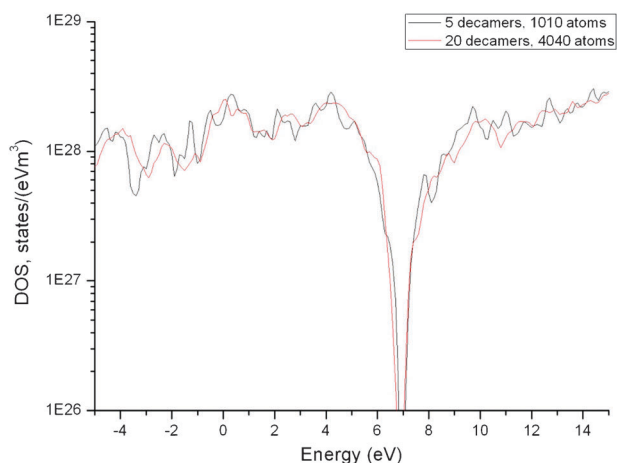


Fig. 3 The dependence of the density of states (states/eV m³, logarithmic scale) on energy in the case of (a) 5 decamers and (b) 20 decamers.

1.107 g cm⁻³, the same as the 5 chain case. The atomic structures of both systems after minimization to a local minimum are shown in Fig. 2 (molecular graphics images were produced using the UCSF Chimera package from the Resource for Biocomputing, Visualization, and Informatics at the University of California, San Francisco).³² The DOSs of each system calculated using the generalized moments method³³ implemented in the Escan code are shown in Fig. 3. Since there is a close similarity between the densities of states of the two systems, the smaller 1010 atom system was chosen as being representative of an infinite amorphous system in the following analysis.

3.2. Eigenfunctions of the amorphous system

To gain insight into the electronic structure of the amorphous systems, we calculated several wave functions near the top of the valence band and the bottom of the conduction band. Valence band states are always localized on the interring C≡C triple bond, never localized on a sulfur atom. They are also localized in varying degrees on the phenyl and thiadiazole rings. Conduction band states, on the other hand, are always localized on both the interring C–C single bonds and the sulfur atom (see Fig. 4). Therefore, valence and conduction band states resemble the HOMO and the LUMO levels, respectively, of a planar PhEtTh oligomer (see Fig. 2S in the ESI†). All of these are in agreement with our previous calculations on single chains and molecules using the B3LYP/6-31G* method. However, there are important differences that appear when comparing eigenfunctions of the whole amorphous system to both each individual chain within the amorphous system and to a planar oligomer.

As already mentioned, the π -conjugation of these systems is expected to be maintained to varying degrees between adjacent aryl groups at different relative orientations.^{12–17} Although it is clear that eigenfunctions belonging to the amorphous PhEtTh oligomer are more localized than those of the planar oligomers, we can conclude that, indeed, the axial symmetry of the triple bond allows π -conjugation to extend for dihedral

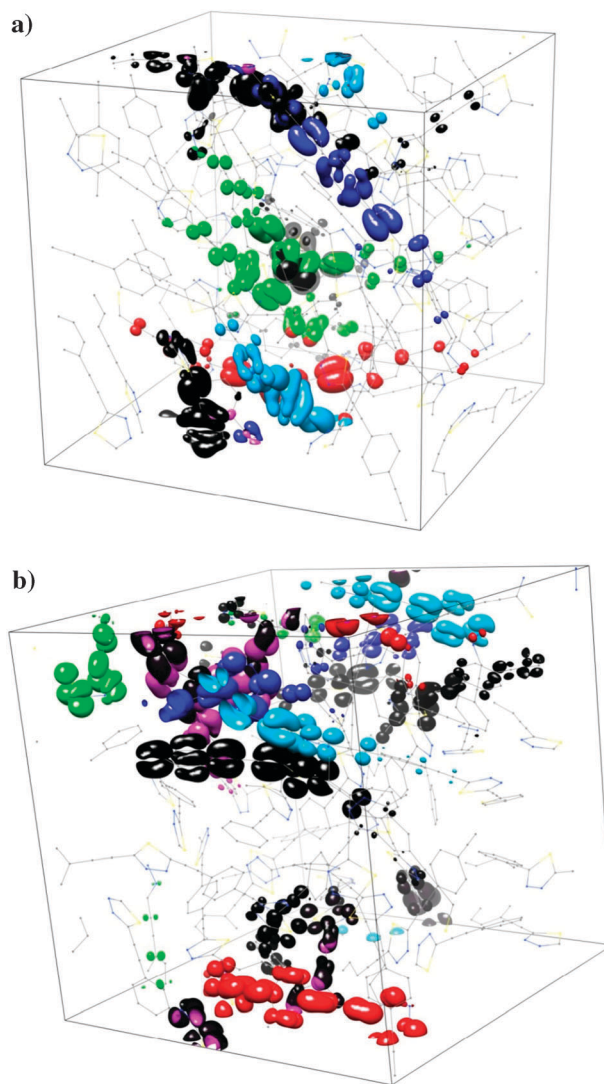


Fig. 4 Isosurface plots of the amorphous system wavefunctions. Isosurfaces correspond to a 50% probability of finding an electron inside the surface. The atomic structure of each chain is also shown, although hydrogen atoms have been removed for clarity. (a) The last six states in the valence band. (b) The first seven states in the conduction band. Isosurfaces are colored as follows: HOMO or LUMO dark blue, HOMO–1 or LUMO+1 green, HOMO–2 or LUMO+2 light blue, HOMO–3 or LUMO+3 red, HOMO–4 or LUMO+4 pink, HOMO–5 or LUMO+5 black, and HOMO–6 or LUMO+6 grey.

angles up to $\sim 50^\circ$. Also, despite there being some resemblance between the amorphous system states and those corresponding to each individual oligomer within the amorphous system (calculated in isolation with no influences of the other chains while retaining its geometry inside the amorphous system), one important difference is that one can find eigenfunctions that spread over 2 chains (in the case of the valence band, see Fig. 5) and even over 4 chains (in the case of the conduction band, see Fig. 3S in the ESI†). Fig. 5 shows how the HOMO–1 of the whole amorphous system could be described as a linear combination of an HOMO of one isolated oligomer and the HOMO–1 of another. Despite this similarity between

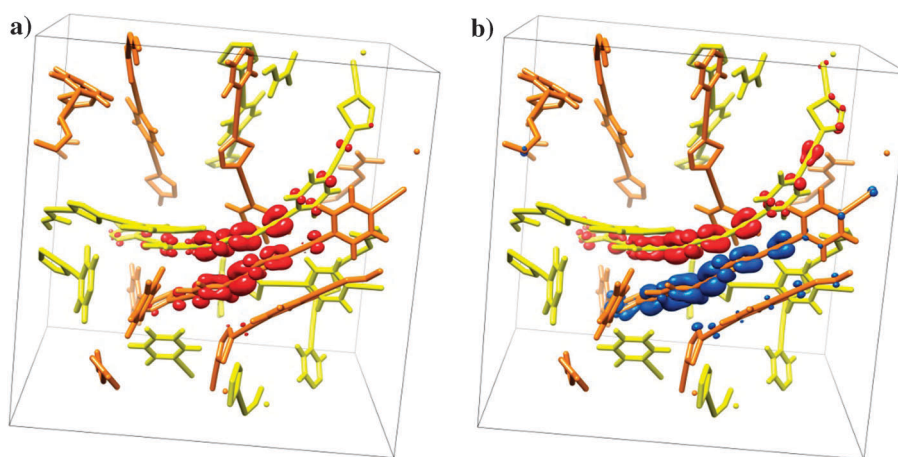


Fig. 5 Isosurface plots (50% of probability of finding an electron inside each surface) of (a) the HOMO–1 of the whole amorphous system, and (b) the HOMO of one isolated oligomer (red) together with the HOMO–1 of another isolated oligomer (blue). The atoms of each oligomer have been colored differently.

eigenfunctions corresponding to the whole system and the isolated oligomer chains, as shown in Fig. 5, in general there is no direct correspondence between them, as they might localize at different places (see Fig. 4S in the ESI†). These observations suggest that there is a strong interaction between the chains, and that the electronic structure of the whole system cannot be understood as a simple collection of the electronic structures of isolated individual chains. Although the carrier mobility in such an amorphous system is complicated, and accurate values could only be attained after electron–phonon interactions are taken into account,²⁵ the strong interchain coupling and the spreading of the wavefunctions into multiple chains can help to increase the carrier mobility according to the following two factors. First, the hopping rates between neighboring states will be increased as the wavefunction overlap increases.³⁴ Second, during the molecular dynamics of the amorphous system, the coupling between neighboring chains might change in a random way and, as a result, the adiabatic eigenstates might change dramatically in terms of the wavefunction spreading crossing multiple chains. This will give rise to a dynamic contribution to the carrier mobility.³⁵ Another major factor for carrier transport is the tail DOSs at the band edges. This will be discussed later.

To gain an understanding of the nature of the above interchain interaction, we have calculated the electronic structure of each isolated individual chain. Table 1S in the ESI† shows the calculated eigenvalues and the band gaps together with those obtained for the whole amorphous system. The calculated band gap of disordered poly-PhEtTh is 0.62 eV, while the band gap for each chain lies in the range of 1.60–1.85 eV. All the calculations are based on LDA, and therefore results are susceptible to the well-known LDA band gap problem.³⁶ It is, however, a common procedure for these polymer systems to increase the LDA band gap values by a factor of 1/0.60³⁷ to allow comparisons with experimental data. In this way, band gap values for individual chains can, to some extent, be compared to the experimental band gap of 2.81 eV of poly-2-(2,5-bis-didodecyloxy-4-ethynylphenylethynyl)-1,3,4-thiadiazole,⁷ measured in CHCl₃ solution. Hence, the

band gap values calculated for each individual chain are reasonable and their calculated densities of states (see Fig. 1S in the ESI†) are quite similar. Note that when calculated in isolation, their energy levels are relatively aligned among different chains, as shown in Fig. 1S and Table 1S in the ESI†. Thus, if we took the electronic structure of the whole system as a collection of the electronic structures of the isolated individual chains, then the band gap of the whole system would also be in the range of 1.60–1.85 eV, not the 0.62 eV as directly calculated. The striking difference of the band gap between the individual chains and for the whole amorphous system indicates possible strong interactions between the chains, as can be shown by both the coupling integral t_{ij} (eqn (1)), and a long range electrostatic interaction which causes the local electrostatic potential to fluctuate. Further discussion (in section 3.5) will shed light on the role of both of these effects. The above difference between the individual chains and the whole amorphous system is also an indication that there could be relatively long DOS tails near the band edge (imagining that the total DOS is a sum of individual chain DOSs plus some random energy shifts), although much larger systems and more statistics are needed to figure out the detailed shapes of the DOS tails (which is beyond the scope of the current study). These long DOS tails can significantly diminish the hopping related carrier transport. This is in sharp contrast with the polythiophenes,^{20,25} where it was found that the electronic structure of the whole system can be approximated as the sum of the electronic structures of individual chains.

3.3. Eigenfunctions of an ideal ordered system

In order to check the influence of disorder and chain twisting on the eigenstates of the real system, a reference, ideal, system will be very useful. Thus, we have analyzed a model system consisting of two planar cofacial PhEtTh oligomers ($n = 10$) separated from each other by a variable distance from 3–5 Å, in steps of 0.5 Å. Table 3 shows that band gaps for an individual, perfectly planar, oligomer are quite similar to those

Table 3 Calculated eigenvalues and band gaps (in eV) for a system composed of 2 planar parallel PhEtTh oligomers ($n = 10$)

| Separation | HOMO | LUMO | Band gap |
|------------|--------|--------|----------|
| 3.0 Å | -3.887 | -3.668 | 0.22 |
| 3.5 Å | -4.263 | -3.322 | 0.94 |
| 4.0 Å | -4.449 | -3.165 | 1.28 |
| 4.5 Å | -4.551 | -3.108 | 1.44 |
| 5.0 Å | -4.615 | -3.097 | 1.52 |
| Infinity | -5.154 | -3.512 | 1.64 |

obtained for an isolated twisted one (*i.e.* extracted from the whole amorphous system; compare Table 3 with Table 1S in the ESI†). The twisted one has a slightly larger band gap, due to the quantum confinement effect in the chain direction. The band gap decreases from the single oligomer chain to the two oligomer system due to the *inter* oligomer electron coupling. Its implication for band gap reduction for the amorphous system will be discussed in the following subsections. The calculated HOMO and LUMO can be visualized in Fig. 2S in the ESI†. As can be seen, the HOMO is more localized at the center, while the LUMO spreads over more monomer units with a weak amplitude at the middle of the chain.

3.4. Electronic coupling

As shown above, the electronic coupling between chains can have a strong influence on the overall electronic structure of the system. Furthermore, it determines the electron transfer rate between the chains and, consequently, can have a major impact on electric transport within the system.

We have thus explicitly calculated the electronic coupling elements (t_{ij}) between the orthonormalized wavefunctions i and j , when they are on different chains or on the same chain (which we will call *off diagonal intrachain elements*). Tables 2S–3S and 4S–5S in the ESI† show the highest calculated interchain electronic couplings (absolute value) for the amorphous system and for the two planar cofacial PhEtTh oligomers ($n = 10$) discussed in section 3.3, respectively. For the amorphous system, the highest interchain t_{ij} value is about 40 meV among conduction states, and 25 meV among valence states. On the other hand, in the case of two planar cofacial oligomers, the highest interchain coupling is about 300 meV for conduction states and 200 meV for valence states at a distance of 3.5 Å, which is close to the average interchain distance in the amorphous system. These values are clearly larger than those obtained in the case of the amorphous system.

It has recently been pointed out that when several nearly-degenerate states appear near the gap, averaging over these states should be used to estimate coupling.³⁸ Hence, an effective coupling squared can be estimated as

$$\langle t \rangle^2 = N_2 (t^{\text{rms}})^2 \quad (2)$$

$$t^{\text{rms}} = \sqrt{\frac{1}{N_1 N_2} \sum_{i=1}^{N_1} \sum_{j=1}^{N_2} t_{ij}^2} \quad (3)$$

where N_1 and N_2 are the numbers of (nearly) degenerate states localized on each chain. We have chosen $N_1 = N_2$, being the number of states lying within a gap of ~ 0.3 eV. Hence N_2 in

Table 4 Average effective couplings (in meV) between chains of the amorphous system

| Chain_m/Chain_n | Conduction band | Valence band |
|-----------------|-----------------|--------------|
| 1/2 | 11.0 | 15.7 |
| 1/3 | 24.0 | 14.4 |
| 1/4 | 11.4 | 6.6 |
| 1/5 | 15.2 | 10.6 |
| 2/3 | 11.4 | 7.0 |
| 2/4 | 14.3 | 9.0 |
| 2/5 | 8.7 | 12.6 |
| 3/4 | 25.7 | 13.6 |
| 3/5 | 9.1 | 5.6 |
| 4/5 | 6.7 | 2.5 |

Table 5 The average effective couplings between two planar cofacial PhEtTh oligomers ($n = 10$), in meV

| Chain separation | $\langle t \rangle$ | | | | |
|------------------------|---------------------|-------|-------|-------|------|
| | 3 Å | 3.5 Å | 4 Å | 4.5 Å | 5 Å |
| Conduction band | 506.0 | 246.6 | 124.0 | 49.4 | 25.4 |
| Valence band | 325.6 | 200.0 | 81.7 | 30.0 | 10.6 |

eqn (2) can be thought of as the number of pathways for the electron (hole) going from one chain to another. Tables 4 and 5 show the averaged, effective couplings between chains for the amorphous system and two planar, cofacial PhEtTh oligomers, respectively. On the other hand, Table 6 shows the corresponding effective average for the off diagonal intrachain elements calculated in the same way as above for states within 0.3 eV near the band edges.

We first discuss the consequences of interchain effective coupling elements in terms of the charge transport in the system. The typical interchain distance in the amorphous system is between 3.5–4 Å. The effective coupling for two planar cofacial oligomers at that distance is still an order of magnitude larger than the effective coupling in an amorphous system, as can be seen in Tables 4 and 5. The reason for the difference is probably due to the reduced physical contact area in the amorphous system and the mismatch between the contact areas and the places of localizations of the band edge wave functions. The decrease of the interchain electronic coupling in the amorphous system will certainly have a detrimental effect on the electrical transport.

3.5. The model of electronic structure of the amorphous system

As we have seen previously, the interchain electronic coupling elements in the amorphous systems are generally rather small (of the order of 10 meV) which indicates that the electronic coupling cannot explain the large band gap reduction in the

Table 6 The average effective off diagonal intrachain elements (meV)

| Chain | Conduction band | Valence band |
|-------|-----------------|--------------|
| 1 | 225.4 | 3.0 |
| 2 | 48.7 | 129.4 |
| 3 | 69.2 | 106.8 |
| 4 | 44.9 | 66.5 |
| 5 | 69.4 | 88.5 |

Table 7 Calculated eigenvalues and band gaps (in eV) of the whole amorphous system. Column (a) shows the eigenvalues for the whole system calculated with the ESCAN code; column (b) the eigenvalues in the basis of wavefunctions of single chains; column (c) the eigenvalues after turning off interchain coupling elements; and column (d) the eigenvalues after also turning off the off diagonal intrachain elements

| | (a) | (b) | (c) | (d) |
|-------------|--------------|--------------|--------------|--------------|
| LUMO+7 | 7.580 | 7.587 | 7.592 | 7.689 |
| LUMO+6 | 7.556 | 7.558 | 7.508 | 7.685 |
| LUMO+5 | 7.442 | 7.468 | 7.497 | 7.672 |
| LUMO+4 | 7.417 | 7.438 | 7.464 | 7.593 |
| LUMO+3 | 7.397 | 7.433 | 7.425 | 7.529 |
| LUMO+2 | 7.344 | 7.402 | 7.417 | 7.515 |
| LUMO+1 | 7.329 | 7.379 | 7.383 | 7.509 |
| LUMO | 7.251 | 7.347 | 7.349 | 7.414 |
| HOMO | 6.627 | 6.555 | 6.548 | 6.409 |
| HOMO−1 | 6.509 | 6.413 | 6.301 | 6.247 |
| HOMO−2 | 6.435 | 6.272 | 6.268 | 6.214 |
| HOMO−3 | 6.394 | 6.217 | 6.247 | 6.194 |
| HOMO−4 | 6.325 | 6.212 | 6.198 | 6.036 |
| HOMO−5 | 6.306 | 6.173 | 6.160 | 6.011 |
| HOMO−6 | 6.291 | 6.122 | 6.116 | 6.005 |
| HOMO−7 | | 6.069 | 6.086 | 5.975 |
| Band gap | 0.62 | 0.79 | 0.80 | 1.01 |

amorphous system, in contrast to the case of two parallel oligomers discussed in subsection 3.3, where the band gap reduction can be explained by interchain coupling. In order to shed light on the factors that determine the electronic structure and, consequently, the band gap, we have performed several additional calculations that are summarized in Table 7. In these calculations we represent the Kohn–Sham Hamiltonian of the whole system in the basis of eigenstates of single chains by forming the matrix elements $H_{ij} = \langle i|H|j \rangle$ and $S_{ij} = \langle i|j \rangle$ (where $|i \rangle$ and $|j \rangle$ are the previously calculated wavefunctions of single chains). This basis is convenient, as we can easily turn on or turn off certain coupling elements and therefore understand how they impact the electronic structure of the system. The eigenvalues of the Hamiltonian are found by solving the generalized eigenvalue problem, *i.e.* $\det(H - ES) = 0$.

To check the quality of the basis set used, we first perform the calculation with all coupling elements turned on. As the basis set used is not complete, the results differ to some extent from the ESCAN direct plane wave basis set calculation for the whole amorphous system (see Table 7). As can be seen, the differences are small (~ 0.1 eV), thus this basis set can be used for comparison purposes to understand the role of different coupling elements. The calculated band gap with this basis set is 0.79 eV. Next, we solve the eigenvalue problem again, but with interchain H_{ij} and S_{ij} elements turned off. This way, we measure the effect of the interchain coupling, which, as expected from $\langle i|j \rangle$ values, is very small (there is a change in band gap from 0.79 to 0.80 eV). Finally, we calculate the eigenvalues when we also turn off the H_{ij} and S_{ij} $i \neq j$, elements with i and j originating from the same chain. As could also be expected from the corresponding average effective off diagonal intrachain elements, this has a more pronounced effect on the electronic structure, and the band gap increases up to 1.01 eV. Furthermore, if we also ignore the onsite coupling term $(H - H_{\text{single}})_{ii}$, we reduce down to the single chain band gaps,

and in that case, the band gap rises up to 1.60–1.85 eV (Table 1S in the ESI†).

These calculations allow us to give a detailed description of the factors that determine the electronic structure of the amorphous system. Individual isolated chains have band gaps in the 1.60–1.85 eV region. The long range electrostatic potential caused by the presence of other chains leads to changes in onsite energies H_{ii} , and consequently to a band gap reduction to 1.01 eV, as shown in Table 7(d). The electrostatic potential also mixes different states within an isolated chain and causes the observed relocation of the localized states, as can be expected from the relatively high values of the intrachain effective coupling elements in Table 6. This leads to a further reduction of the band gap (Table 7(c)) from 1.01 to 0.8 eV. Finally, electronic coupling between different chains is weak and has a minor effect on the band gap. Nevertheless, it can occasionally hybridize the states of different chains and cause the wavefunction to be delocalized over two or more chains, as shown in Fig. 5(a).

These results suggest that the disordered electrostatic potential caused by the presence of other chains has a profound effect on the electronic properties of amorphous PhEtTh polymer materials, as it significantly reduces the band gap of the material. On the other hand, in our previous study of polythiophene materials²³ no such large effect was observed for the band gap, although it might still be a major cause of wavefunction localization and the shape of the band edge DOS tails. The main difference between these two classes of materials comes from the fact that the repeat unit of poly-PhEtTh has a significant dipole moment that originates from a charge transfer of 0.14 electrons (as obtained from DFT calculations) from thiadiazole to benzene ring. This dipole moment induces long range electrostatic interactions. As a consequence, a stronger interchain electrostatic interaction is formed in PhEtTh materials compared to polythiophenes, where there is no large dipole moment due to their single ring polymer repeat unit.

This band gap reduction in the amorphous region of the material may possibly even alter the energy level alignment between the amorphous and ordered region of the material. A typical situation in polymer materials is that electronic coupling between the chains in the ordered regions decreases the band gap of the polymer (in comparison to an isolated polymer chain), while quantum confinement in the disordered regions increases the band gap. For these reasons, one usually argues that the band gap of the ordered region is smaller than the one of the amorphous region. The carriers then reside in ordered regions. If the relative content of ordered regions is sufficiently high to form a percolating network, transport in the material is determined by the ordered regions. However, in our case the band gap reduction of the amorphous material caused by long range electrostatic interactions may completely alter this picture and cause the band gap of the amorphous region to be smaller than the band gap of the ordered material. The carriers would then reside in the amorphous material and the transport would be entirely determined by the amorphous regions, despite the presence of ordered regions. A full understanding of this effect would,

however, require the study of the interface of the ordered and disordered region of the polymer material, which is beyond the scope of the current study.

4. Conclusions

We calculated the electronic structure of amorphous PhEtTh polymer materials and the electronic coupling between polymer chains using the charge patching method, and compared the results with polythiophene systems. We found the following conclusions. (1) The CPM works slightly worse in this system compared to the polythiophene system, because there are larger long range electric fields and we have not included the bond length and angle derivative motifs. (2) The electronic structure of the whole disordered system cannot be viewed as a simple collection of the electronic structures of isolated individual chains. There is a strong coupling (both electronic and electrostatic) between different chains. This is in contrast with the polythiophene system. (3) The whole disordered system has a band gap ~ 1.0 eV smaller than the band gap of individual isolated chains (with chain geometry taken from the disordered system). (4) There are three types of coupling: interchain electronic coupling; intrachain off diagonal electronic coupling; and intrachain onsite electronic coupling (the onsite potential perturbation caused by the interchain electrostatic coupling). The interchain coupling has a very minimal (~ 10 meV) effect on the band gap; the intrachain coupling reduces the band gap by about 0.1 eV, and it also causes re-localization of the electron states. The biggest band gap reduction comes from onsite potential fluctuation, which is caused by interchain electrostatic interactions. (5) The interchain electronic coupling for the amorphous PhEtTh system is one order of magnitude smaller than the ordered cofacial stacking system with a similar interchain distance. This will have a negative effect on the electrical transport throughout the system. Nevertheless, the wavefunctions can be spread out across multiple chains. (6) While a much larger system and statistics would be required to obtain reliable information about the shape of the DOS tail near the band edge,³⁹ it is reasonable to deduce that the reduction of the band gap in the disordered system means long DOS tails at both sides of the band gap. Because the hopping mobility of a disordered system depends sensitively on the width of these DOS tails, this will significantly reduce carrier mobility in the system. In comparison, the polythiophene disordered system does not have this large reduction of the band gap. (7) Since the large band gap reduction in PhEtTh is caused by the electrostatic interchain interaction, which, in turn, is caused by the large ring-to-ring dipole in PhEtTh, we thus propose that, as a design principle to achieve large mobility in a disordered polymer system, one should minimize the dipole moment in the polymer repeat unit.

Acknowledgements

JMFR and MFG gratefully acknowledge Consejería de Innovación, Ciencia y Empresa, Junta de Andalucía (PAI-FQM 337 contract and FQM-P06-01864) for financial support.

NV and LWW were supported by the SC/BES/DMSE of the U.S. Department of Energy under Contract No. DE-AC02-05CH11231. The resources of National Energy Research Scientific Computing Center (NERSC) were used. In the last stages of this work, NV was supported by the Ministry of Science and Technological Development of the Republic of Serbia, under project No. ON171017 and the European Commission under EU FP7 projects PRACE-IIP, HP-SEE and EGI-InSPIRE.

Notes and references

- 1 *Handbook of Conducting Polymers, Conjugated Polymers, Theory, Synthesis, Properties, and Characterization*, ed. T. A. Skotheim and J. R. Reynolds, 3rd edn, 2007.
- 2 V. Coropceanu, J. Cornil, D. A. da Silva Filho, Y. Olivier, R. Silbey and J. L. Bredas, *Chem. Rev.*, 2007, **107**, 926–952.
- 3 I. McCulloch, *Nat. Mater.*, 2005, **4**, 583–584.
- 4 J. Nelson, *Curr. Opin. Solid State Mater. Sci.*, 2002, **6**, 87–95.
- 5 H. E. Katz, *Chem. Mater.*, 2004, **16**, 4748–4756.
- 6 R. A. Street, J. E. Northrup and A. Salleo, *Phys. Rev. B: Condens. Matter Phys.*, 2005, **71**, 165202.
- 7 T. Yasuda, T. Imase, Y. Nakamura and T. Yamamoto, *Macromolecules*, 2005, **38**, 4687–4697.
- 8 E. Jansson, P. C. Jha and H. Aagren, *Chem. Phys.*, 2006, **330**, 166–171.
- 9 D. Glossman-Mitnik, *THEOCHEM*, 2001, **549**, 285–288.
- 10 N. Flores-Holguin and D. Glossman-Mitnik, *THEOCHEM*, 2003, **634**, 67–76.
- 11 M. Sato, Y. Tada, S. Nakashima, K. I. Ishikura, M. Handa and K. Kasuga, *J. Polym. Sci., Part A: Polym. Chem.*, 2005, **43**, 1511–1525.
- 12 A. Beeby, K. S. Findlay, P. J. Low, T. B. Marder, P. Matousek, A. W. Parker, S. R. Rutter and M. Towrie, *Chem. Commun.*, 2003, 2406–2407.
- 13 A. Beeby, K. Findlay, P. J. Low and T. B. Marder, *J. Am. Chem. Soc.*, 2002, **124**, 8280–8284.
- 14 S. J. Greaves, E. L. Flynn, E. L. Fitcher, E. Wrede, D. P. Lydon, P. J. Low, S. R. Rutter and A. Beeby, *J. Phys. Chem. A*, 2006, **110**, 2114–2121.
- 15 M. Levitus, K. Schmieder, H. Ricks, K. D. Shimizu, U. H. F. Bunz and M. A. Garcia-Garibay, *J. Am. Chem. Soc.*, 2001, **123**, 4259–4265.
- 16 J. M. Granadino-Roldan, A. Garzon, G. Garcia, T. Pena-Ruiz, M. P. Fernandez-Liencres, A. Navarro and M. Fernandez-Gomez, *J. Chem. Phys.*, 2009, **130**, 234907.
- 17 A. Garzon, J. M. Granadino-Roldan, M. Moral, G. Garcia, M. P. Fernandez-Liencres, A. Navarro, T. Pena-Ruiz and M. Fernandez-Gomez, *J. Chem. Phys.*, 2010, **132**, 064901.
- 18 L. W. Wang, *Annu. Rev. Phys. Chem.*, 2010, **61**, 19–39.
- 19 N. Vukmirovic and L. W. Wang, *J. Chem. Phys.*, 2008, **128**, 121102.
- 20 <https://hpcrd.lbl.gov/~linwang/PEtot/PEtot.html>.
- 21 L. W. Wang and A. Zunger, *J. Chem. Phys.*, 1994, **100**, 2394–2397.
- 22 A. Canning, L. W. Wang, A. Williamson and A. Zunger, *J. Comput. Phys.*, 2000, **160**, 29–41.
- 23 N. Vukmirovic and L. W. Wang, *J. Phys. Chem. B*, 2009, **113**, 409–415.
- 24 L. W. Wang, *Phys. Rev. B*, 2002, **65**, 1534101–1534104.
- 25 N. Vukmirovic and L. W. Wang, *Nano Lett.*, 2009, **9**, 3996–4000.
- 26 L. W. Wang and X. Cartoixà, *Phys. Rev. B: Condens. Matter Phys.*, 2007, **75**, 205334.
- 27 G. Zhang, J. Ma and J. Wen, *J. Phys. Chem. B*, 2007, **111**, 11670–11679.
- 28 H.-C. Yang, C.-Y. Hua, M.-Y. Kuo, Q. Huang and C.-L. Chen, *ChemPhysChem*, 2004, **5**, 373–381.
- 29 S. Plimpton, *J. Comput. Phys.*, 1995, **117**, 1–19.
- 30 H. Sun and D. Rigby, *Spectrochim. Acta, Part A*, 1997, **53**, 1301–1323.
- 31 P. O. Löwdin, *J. Chem. Phys.*, 1950, **18**, 365–375.

-
- 32 E. F. Pettersen, T. D. Goddard, C. C. Huang, G. S. Couch, D. M. Greenblatt, E. C. Meng and T. E. Ferrin, *J. Comput. Chem.*, 2004, **25**, 1605–1612.
- 33 L. W. Wang, *Phys. Rev. B: Condens. Matter*, 1994, **49**, 10154–10158.
- 34 N. Vukmirovic and L. W. Wang, *Appl. Phys. Lett.*, 2010, **97**, 043305–043303.
- 35 D. P. McMahon and A. Troisi, *ChemPhysChem*, 2010, **11**, 2067–2074.
- 36 A. Seidl, A. Görling, P. Vogl, J. A. Majewski and M. Levy, *Phys. Rev. B: Condens. Matter*, 1996, **53**, 3764.
- 37 G. Brocks, P. J. Kelly and R. Car, *Synth. Met.*, 1993, **57**, 4243–4248.
- 38 A. A. Voityuk, *Chem. Phys. Lett.*, 2010, **495**, 131–134.
- 39 N. Vukmirovic and L. W. Wang, *J. Phys. Chem. B*, 2011, **115**, 1792–1797.